AGU PUBLICATIONS

Global Biogeochemical Cycles

RESEARCH ARTICLE
10.1002/2014GB005051

Key Points:
- Little nitrate consumption in an iron-fertilized bloom of the Southern Ocean
- Significant mixed layer nitrification
- Nitrate-based primary production is mainly regenerated production

Supporting Information:
- Text S1
- Figures S1–S5

Correspondence to:
F. Fripiat,
ffripiat@vub.ac.be

Citation:
Fripiat, F., et al. (2015), Significant mixed layer nitrification in a natural iron-fertilized bloom of the Southern Ocean, *Global Biogeochem. Cycles*, *29*, 1929–1943, doi:10.1002/2014GB005051.

Received 2 DEC 2014
Accepted 19 OCT 2015
Accepted article online 21 OCT 2015
Published online 20 NOV 2015

Significant mixed layer nitrification in a natural iron-fertilized bloom of the Southern Ocean

F. Fripiat[1], M. Elskens[1], T. W. Trull[2], S. Blain[3], A.-J. Cavagna[1], C. Fernandez[3], D. Fonseca-Batista[1], F. Planchon[4], P. Raimbault[5], A. Roukaerts[1], and F. Dehairs[1]

[1]Analytical, Environmental, and Geochemistry, Earth Sciences Research Group, Vrije Universiteit Brussel, Brussels, Belgium, [2]Antarctic Climate and Ecosystems Cooperative Research Centre, University of Tasmania and CSIRO Oceans and Atmosphere Flagship, Hobart, Australia, [3]CNRS, Laboratoire d'Océanographie Microbienne, Observatoire Océanologique, Sorbonne Universités, UPMC Univ Paris 06, Banyuls sur Mer, France, [4]Laboratoire des Sciences de l'Environment Marin, Institut Européen de la Mer, Plouzané, France, [5]CNRS/INSU, IRD, Mediterranean Institute of Oceanography UMR 7294, Aix-Marseille Université, Marseille, France

Abstract Nitrification, the microbially mediated oxidation of ammonium into nitrate, is generally expected to be low in the Southern Ocean mixed layer. This paradigm assumes that nitrate is mainly provided through vertical mixing and assimilated during the vegetative season, supporting the concept that nitrate uptake is equivalent to the new primary production (i.e., primary production which is potentially available for export). Here we show that nitrification is significant (~40–80% of the seasonal nitrate uptake) in the naturally iron-fertilized bloom over the southeast Kerguelen Plateau. Hence, a large fraction of the nitrate-based primary production is regenerated, instead of being exported. It appears that nitrate assimilation (light dependent) and nitrification (partly light inhibited) are spatially separated between the upper and lower parts, respectively, of the deep surface mixed layers. These deep mixed layers, extending well below the euphotic layer, allow nitrifiers to compete with phytoplankton for the assimilation of ammonium. The high contributions of nitrification to nitrate uptake are in agreement with both low export efficiency (i.e., the percentage of primary production that is exported) and low seasonal nitrate drawdown despite high nitrate assimilation.

1. Introduction

Southern Ocean biogeochemical cycles play a disproportionate role in setting the air-sea balance of CO_2 and global biological production [*Sarmiento et al.*, 2004; *Sigman et al.*, 2010]. Deep nutrient-rich waters ascend to the surface and are returned as subsurface waters further north, before the available nutrient pools can be fully utilized by phytoplankton [*Sarmiento et al.*, 2004]. This inefficiency of the biological pump to strip nutrients from the surface layer has been attributed to iron and light co-limitation [*Martin et al.*, 1990; *Mitchel et al.*, 1991] and represents (i) a missed opportunity to sequester more CO_2 into the deep ocean [*Sigman et al.*, 2010] and (ii) a nutrient leak toward low-latitude areas [*Sarmiento et al.*, 2004]. In contrast to the dominant high-nutrient low-chlorophyll (HNLC) areas, persistent and large blooms are observed downstream of islands and bathymetric features where the Antarctic Circumpolar Current interacts with topography [*Blain et al.*, 2007; *Sokolov and Rintoul*, 2007], increasing the supply of macro- (e.g., nitrate and phosphate) and micronutrients (e.g., iron).

The largest and recurrent bloom is observed around the Kerguelen Islands and the adjacent plateau to its southeast (Figure 1) [*Blain et al.*, 2007]. The biogeochemical dynamics have been extensively studied during KEOPS 1 and 2 (Kerguelen ocean and plateau compared study) in January–February 2005 and October–November 2011. Despite high primary productivity, the seasonal nitrate (NO_3^-) drawdown was only slightly elevated (6 μmol L^{-1}) in comparison to surrounding HNLC areas (3–4 μmol L^{-1}) [*Pondaven et al.*, 2000; *Nelson et al.*, 2002]. To tackle that apparent paradox, we investigated the upper ocean seasonal nitrogen (N) cycle over the southeast Kerguelen Plateau using model and data for nitrate and ammonium concentrations and uptake rates, particulate nitrogen accumulation and export, and nitrate $\delta^{15}N$ and $\delta^{18}O$ [*Savoye et al.*, 2008; *Trull et al.*, 2008, 2015; *Cavagna et al.*, 2015; *Dehairs et al.*, 2015; *Planchon et al.*, 2015].

We conclude that surface mixed layer nitrification, the microbially mediated process by which ammonium is oxidized to nitrate, contributes significantly to the recycling and supply of nitrate for phytoplankton growth. A mixed layer which extends deeper than euphotic layer allows the nitrate produced by nitrification in the

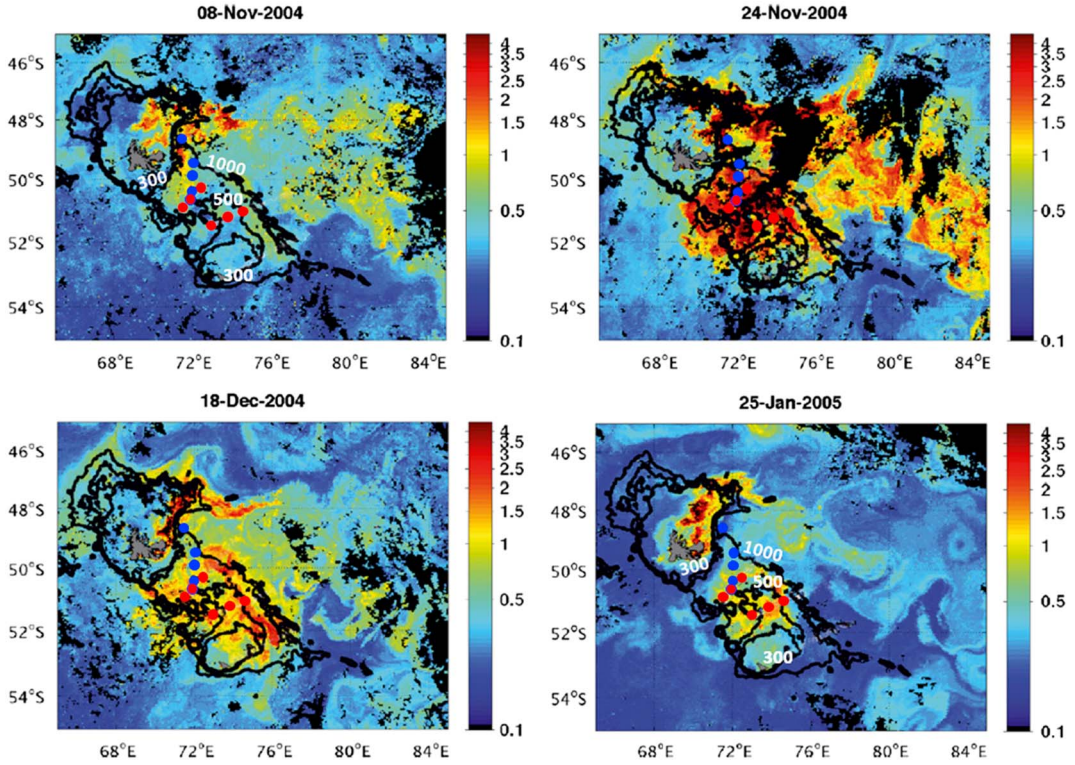

Figure 1. Seasonality of the bloom over and downstream of the Kerguelen Plateau as shown by Moderate Resolution Imaging Spectroradiometer (MODIS) Aqua chl *a* images during the 2005 bloom period. Contours show the bathymetry [300, 500, and 1000 m isobaths; adapted from *Mongin et al.*, 2008]. The red and blue circles show the KEOPS 1 and 2 stations investigated in this study.

aphotic part of the mixed layer (i.e., partly light inhibited) to become directly available for phytoplankton growth in the euphotic layer above. A deep spring-summer mixed layer appears to be a characteristic feature over the Kerguelen Plateau and could explain the high contribution of nitrification to nitrate assimilation there. However, a large-scale comparison between mixed layer depth (MLD) and euphotic layer depth (Z_{eu}) for the open "ice-free" Antarctic zone indicates that such a feature (MLD $> Z_{eu}$) is common in early spring (October–November), likely imposing a tighter coupling between nitrate consuming and regenerating processes for this area in early spring than previously thought.

2. Methods

The southeast Kerguelen Plateau is located south of the Polar Front in the open ice-free Antarctic zone (near 72°E and 51°S). This study combines several data sets obtained during two expeditions to the region that bracketed the seasonal cycle in biomass production (Figure 1). KEOPS 1 was carried out in January–February 2005 and KEOPS 2 in October–November 2011. The data include vertical profiles of nitrate $\delta^{15}N$ and $\delta^{18}O$ [*Trull et al.*, 2008; *Dehairs et al.*, 2015], mixed layer particulate nitrogen (PN) $\delta^{15}N$ [*Trull et al.*, 2008, 2015], NO_3^- and NH_4^+ uptake rates in the 100 and 0.1–0.01% PAR (photosynthetically active radiation) depth ranges [*Cavagna et al.*, 2015; P. Raimbault, unpublished results], and ^{234}Th-based particulate N (PN) export rates [*Savoye et al.*, 2008; *Planchon et al.*, 2015]. The discussion is focused on the southeast Kerguelen Plateau because this area was studied during both the spring and late summer expeditions, allowing us to constrain the seasonal evolution of the N-biogeochemical cycle (from October to February). Specifically we used data from KEOPS 1 stations A1, A3, A5, B1, B3, and B5 and KEOPS 2 stations A3, TNS-8, TNS-9, TNS-10, TEW-4, and E4-W (therefore neglecting the stations outside the Kerguelen Plateau area). This highly productive area is associated with weak mean currents that suggest residence times over the plateau reaching ~7–8 months [*Park et al.*, 2008a, 2008b]. Thus, seasonal changes of water column properties reflect mainly local biogeochemical properties over the vegetative season (~3 months).

Method details for the different parameters are available in the individual publications, so here we provide only a brief overview. Nitrate (NO_3^-), nitrite (NO_2^-), and ammonium (NH_4^+) concentrations were measured on board with an autoanalyzer. PN concentrations (GF/F filtered seawater) were measured with an elemental analyzer–isotope ratio mass spectrometry (EA-IRMS). Uptake rates were measured using shipboard incubations of ^{15}N and ^{13}C tracers (NO_3^-, NH_4^+, and dissolved inorganic carbon) during KEOPS 1 [P. Raimbault, unpublished results] and KEOPS 2 [*Cavagna et al*., 2015] using the same methods. Seawater was sampled between 100 and 0.1–0.01% PAR, spiked with $H^{13}CO_3^-$ and either ^{15}N-NO_3^- or ^{15}N-NH_4^+, shielded with neutral density screens simulating in situ PAR, and incubated at the temperature of local surface water in a flow-through on-deck incubator (during 24 h). The ^{15}N and ^{13}C incorporation into particulate matter was measured with an EA-IRMS, and uptake rates were computed by solving the mass and isotopic balances in the time frame of the incubations.

PN export rates at 100 m were estimated by *Savoye et al*. [2008] and *Planchon et al*. [2015] for KEOPS 1 and 2, respectively. These studies used the measurement of the natural radioisotope ^{234}Th produced from the decay of ^{238}U. The ^{234}Th is quickly adsorbed onto particles, while ^{238}U remains in solution. Because of its short half-life (24.1 days) and its strong adsorption onto particles, the deficit of ^{234}Th with respect to ^{238}U in the upper layer provides an estimate of the export of particulate matter from the upper ocean [*Buesseler et al*., 2006]. Sparser observations of PN export using free drifting sediment traps gave similar results [*Trull et al*., 2008; *Laurenceau et al*., 2015].

The $\delta^{15}N$ and $\delta^{18}O$ results for the combined pool of $NO_3^- + NO_2^-$ were reported in *Trull et al*. [2008] and *Dehairs et al*. [2015], for KEOPS 1 and 2, respectively, and were measured using the "denitrifier method" [*Sigman et al*., 2001; *Casciotti et al*., 2002]. Briefly 20–30 nmol of $NO_3^- + NO_2^-$ was quantitatively converted to N_2O gas by denitrifying bacteria that lack an active N_2O reductase. The N and O isotopic composition of this N_2O was measured by gas chromatography/isotope ratio mass spectrometry with online cryotrapping. Measurements were referenced to air N_2 and Vienna SMOW using the nitrate reference materials (injected with a NO_3^- concentration of 200 μM): IAEA-N3, with a $\delta^{15}N$ of 4.7‰ and a $\delta^{18}O$ of 25.6‰; USGS-34, with a $\delta^{15}N$ of −1.8‰ and a $\delta^{18}O$ of −27.9‰; and USGS-32, with a $\delta^{15}N$ of 180‰ and a $\delta^{18}O$ of 25.7‰ [*Böhlke et al*., 2003; *Marconi et al*., 2015]. The PN $\delta^{15}N$ for both KEOPS 1 and 2 were measured with an EA-IRMS on suspended PN collected from the mixed layer using high-volume pumps [*Trull et al*., 2008, 2015].

Several recent studies highlight that the inclusion of NO_2^- in measurements of the isotopic composition of $NO_3^- + NO_2^-$ can have a significant impact on the results even if nitrite is present at very low levels [*Casciotti et al*., 2007; *Rafter et al*., 2013; *Fawcett et al*., 2015; *Smart et al*., 2015; see supporting information for a detailed description of this interference]. In the present study, nitrification is inferred from the observed decoupling between N and O isotopes between spring and summer (section 3.2). The sensitivity to possible nitrite interference on this decoupling differs between N and O isotopes and may, therefore, induce a bias. To check whether or not nitrite interference could have induced a significant bias, we tested what would be the effect of varying nitrite $\delta^{15}N$ and $\delta^{18}O$ on the nitrate-only $\delta^{15}N$ and $\delta^{18}O$ (see supporting information). We took into account effects of both the natural variability in nitrite $\delta^{15}N$ and $\delta^{18}O$ and the methodological bias associated with a lower fractional O atom loss when nitrite instead of nitrate is reduced into nitrous oxide prior analysis [*Casciotti et al*., 2007]. From this analysis, it appears that nitrite interference underestimates nitrate $\delta^{15}N$ and $\delta^{18}O$ by 0.3–0.5 ± 0.1‰ and 0.3 ± 0.1‰, respectively. The similar bias for both N and O isotopes implies no significant impact on our assessment of the seasonal decoupling between N and O isotopes (i.e., within the error range of the observations; see supporting information and section 3.2). For this reason and to allow the comparison with both *Trull et al*. [2008] and *Dehairs et al*. [2015], uncorrected $NO_3^- + NO_2^-$ $\delta^{15}N$ and $\delta^{18}O$ values are taken to reflect the NO_3^--only $\delta^{15}N$ and $\delta^{18}O$ values.

The seasonal model is described in detail in the supporting information. The model calculates concentrations and isotopic compositions for the NO_3^-, NO_2^-, NH_4^+, and organic N pools and uses a cost function approach versus observations (that equally weights these pools) to find optimal solutions. It uses the observed fluxes of nitrate and ammonium uptakes, particulate nitrogen export, and upward nitrate supply as additional constraints, with these evaluated over the full seasonal cycle to de-emphasize differences in the effective time scales of these methodologies. The model was run as a single box representing the surface mixed layer to obtain an initial overall perspective on the relative magnitudes of the processes, with a focus on the optimum fit for the ratio of the production of nitrate by nitrification to nitrate uptake. This model was run with and without assumptions regarding dissolved organic nitrogen concentrations (to address dissolved organic

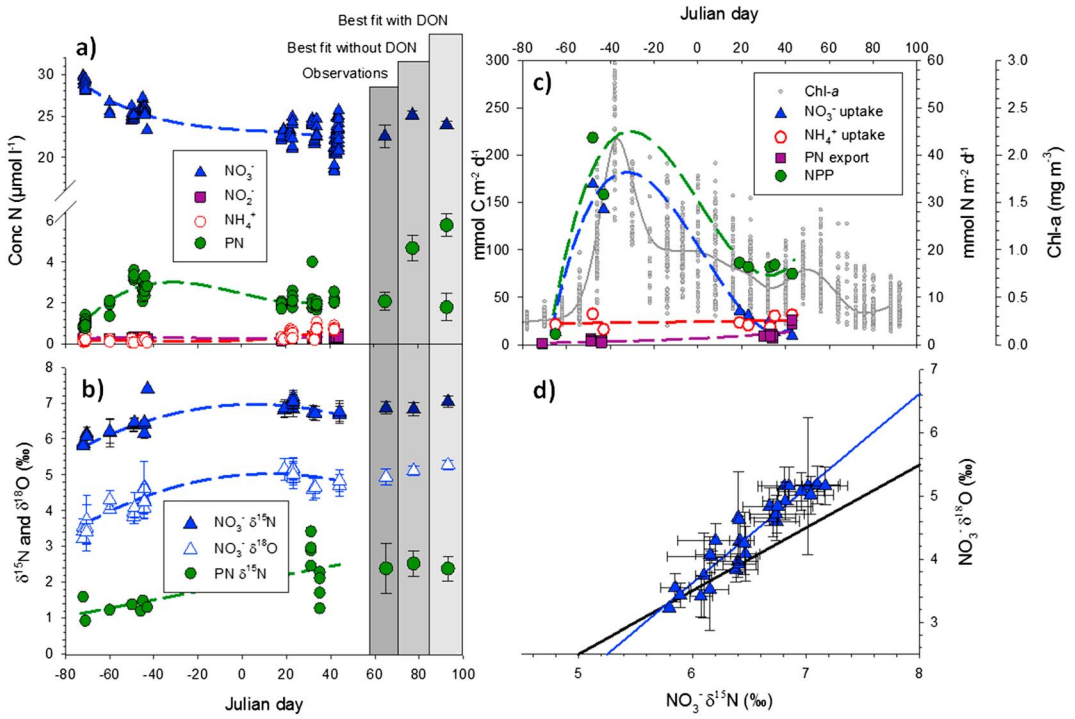

Figure 2. Temporal evolution of rates, concentrations, and isotopic compositions in the mixed layer. (a) Temporal evolution (Julian days versus 31 December; *x* axis) of NO_3^- (blue triangles), NO_2^- (black squares), NH_4^+ (empty red circles), and PN (green circles) concentrations. (b) Temporal evolution of NO_3^- $\delta^{15}N$ (blue filled triangles), NO_3^- $\delta^{18}O$ (blue empty triangles), and PN $\delta^{15}N$ (green circles). (c) Temporal evolution of net primary production (green circles), NO_3^- uptake (blue triangles), NH_4^+ uptake (empty red circles), PN export (purple squares), and MODIS Aqua chl *a* (gray dots, 8 days, 0.25° resolution, between 49.25 and 51.5°S and 71.6 and 73.8°E, available at http://hermes.acri.fr/index.php) [*Maritonera and Siegel*, 2005]. (d) Mixed layer NO_3^- $\delta^{15}N$ versus $\delta^{18}O$ (blue circles, error bar = 1 sd for the replicates, including both early spring and late summer observations). In Figures 2a and 2b, the averages (±sd) of the KEOPS 1 observations are shown in the dark-gray column (i.e., final conditions). The simulations with model outputs falling within ±2 sd of the observations are shown in the medium- and light-gray columns, using model calculations without and with an actively cycling DON pool, respectively. When this pool is incorporated into the model as organic N, the simulated PN concentration (i.e., total organic N minus DON) falls within the error bars of the observations. In Figure 2d, the black line represents the 1:1 reference line (slope of 1) with the initial mixed layer (20 October) as the source and the blue line the data regression line (slope = 1.5 ± 0.1; $R^2 = 0.87$; *P* value < 0.001).

nitrogen (DON) data limitations). A simpler version of this model was also extended to a multibox version to determine the vertical distribution of nitrification, in particular to verify whether the observations required nitrification to occur within the surface mixed layer. Mixed layer (100 ± 40 m; average ± standard deviation (sd) of 56 conductivity-temperature-depth (CTD) profiles during KEOPS 1 and 2) is representative of the surface box in which both primary production and associated N assimilation is occurring. This choice is motivated by the fact that (i) this layer is well mixed with a steep density gradient at the bottom, implying uniform biogeochemical properties and limited exchanges with the underlying ocean, and (ii) the euphotic layer (53 ± 16 m; average ± sd of 21 profiles during KEOPS 1 and 2) in which most of the primary production taking place is more shallow [*Cavagna et al.*, 2015].

3. Results and Discussion

3.1. Biogeochemical Properties

The seasonal evolutions of net primary production and NO_3^- uptake were in agreement with satellite Chl *a* observations (Figures 1 and 2c), which show that the bloom starts in early November, reaches its maximum level in late November–early December, and collapses in January–February [*Blain et al.*, 2007; *Mongin et al.*, 2008; *Cavagna et al.*, 2015].

Deep winter vertical mixing imposed high NO_3^- concentrations in the mixed layer at the onset of the bloom (28.8 µmol L^{-1}; Figures 2a and 3a). Over the course of the bloom nitrate was partly consumed

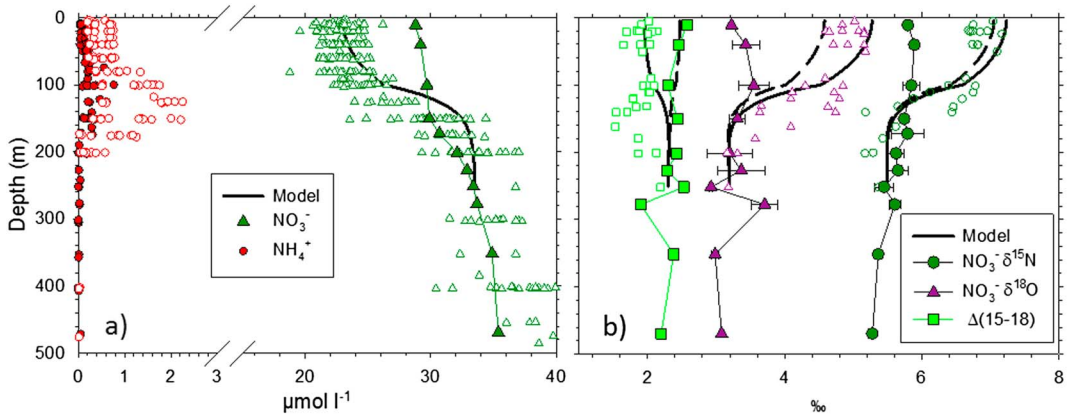

Figure 3. Observed and simulated vertical distributions of concentrations and isotopic compositions. (a) NO_3^- (green triangles) and NH_4^+ (red circles) vertical concentration profiles for the first station (A3-1) of KEOPS 2 (filled symbols; 20 October; representing the initial conditions) and KEOPS 1 (empty symbols; January–February; representing the final conditions). (b) Profiles of NO_3^- $\delta^{15}N$ (green circles), $\delta^{18}O$ (purple triangles), and $\Delta(15–18)$ (green squares) for the first station (A3-1) of KEOPS 2 (filled symbols) and KEOPS 1 (empty symbols). Error bars = 1 sd for the replicates. The black lines represent the final conditions for the time-dependent one-dimensional vertical box model (0–250 m, 50 layers) for nitrification in both the mixed layer and below (full lines) and nitrification exclusively below the mixed layer (dashed lines). The initial model conditions are the first sampled station (A3-1).

with an estimated seasonal NO_3^- drawdown of 0.6 ± 0.2 mol m^{-2}. NO_2^- concentrations in the mixed layer remained relatively low and constant from October to February (0.3 ± 0.1 µmol L^{-1}; Figure 2a). NH_4^+ concentrations increased in the mixed layer from early spring (as low as 0.04 µmol L^{-1}) to late summer (up to 1.05 µmol L^{-1}; Figures 2a and 3a), and a subsurface (150 m) NH_4^+ maximum (up to 2.3 µmol L^{-1}) occurred in late summer (Figure 3a). This maximum coincided with the development of a subsurface Chl *a* maximum [*Mosseri et al.*, 2008] and was located below the mixed layer in the region presenting the highest density gradient. Higher residence times for sinking particles resulting in an accumulation of biomass and associated remineralization is a likely cause of this ammonium peak [*Blain et al.*, 2015].

To compare these seasonal changes in nitrogen concentrations to the daily nitrogen flux measurements, we used the approach of integrating the best fit model curves as shown in Figure 2c. This de-emphasizes the different methodological time scales involved (e.g., 24 h for the uptake incubation experiments and ~30 days for the ^{234}Th-based export estimates) [*Buesseler et al.*, 2006] and yields (with ±90% prediction intervals): NO_3^- uptake = 2.2 ± 1.0 mol m^{-2}, NH_4^+ uptake = 0.5 ± 0.3 mol m^{-2}, and PN export = 0.2 ± 0.2 mol m^{-2}. By comparing the best fit model curves with satellite Chl *a* observations, it is likely that the uptake rates should be in the lower range (Figure 2c). Satellite Chl *a* observations shows a clear spring peak in biomass with less summer continuation. The vertical NO_3^- diffusive flux is also estimated to be 0.2 ± 0.2 mol m^{-2}, from the NO_3^- concentration gradient (5.2 ± 3.4 µmol L^{-1}; between 0–100 and 140–160 m depth stratum) and the estimated vertical diffusivity ($3.0 \pm 1.5 \times 10^{-4}$ m^{-2} s^{-1}) above the southeast Kerguelen Plateau [*Park et al.*, 2008a, 2014].

This comparison shows that on a seasonal basis, primary production was mainly sustained by NO_3^- uptake. Most importantly, even though the seasonally integrated NO_3^- uptake was high, the apparent NO_3^- depletion in the mixed layer over the season remained low (0.6 ± 0.2 mol m^{-2}; Figure 2a). Two processes can be responsible for this imbalance (1.6 mol m^{-2}) between seasonal NO_3^- drawdown and uptake:

1. NO_3^- supply by mixing and/or
2. significant nitrogen remineralization (conversion of particulate nitrogen to ammonium) coupled to nitrification (oxidation of ammonium via nitrite to nitrate).

The mixed layer NO_3^- budget can help to resolve these possible processes and can be described as follows, assuming a negligible contribution of both ammonium and nitrite:

$$\Delta NO_3^- = \Delta ON + ON \text{ export} - NO_3^- \text{supply} \quad (1)$$

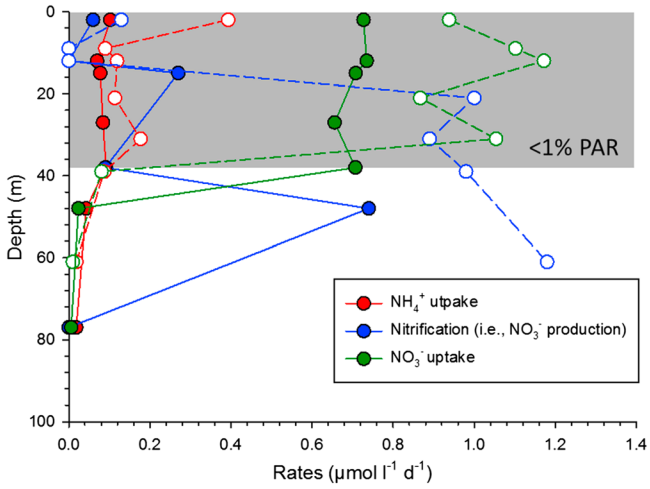

Figure 4. Vertical profiles of key nitrogen cycling rates in the mixed layer (100 ± 40 m) over the Kerguelen Plateau for two stations (A3-2 and E4-W) shown as filled and empty circles for NO_3^- uptake (green symbols), NH_4^+ uptake (red symbols), and nitrification (blue symbols) [*Cavagna et al.*, 2015]. These rates were obtained from ^{15}N isotope enrichment experiments: NO_3^--spiked incubation (24 h) for uptake and nitrification (as reflected in term of production of NO_3^-) and NH_4^+-spiked incubations for NH_4^+ uptake (24 h). The gray zone represents the depths receiving ≥1% of the surface photosynthetically active radiation (i.e., euphotic layer).

where ΔNO_3^- is the apparent NO_3^- depletion, ΔON is the accumulation in the mixed layer of organic N, ON export is the export of organic N below the mixed layer (^{234}Th deficit approach), and NO_3^- supply is the mixing term (=unknown in equation (1)). The accumulation of organic N is based on the PN concentration at the end of the vegetative season (0.21 ± 0.04 mol m^{-2}; Figure 2a) and the dissolved organic N (DON) accumulation (estimated to be 0.4 mol m^{-2} based on observed minus background HNLC concentrations) [*Ogawa et al.*, 1999], although this value is uncertain because DON was only measured during KEOPS 2 [*Blain et al.*, 2015]. Based on these estimates, the mixed layer NO_3^- budget is relatively well balanced (0.6 ± 0.2 versus 0.6 ± 0.3 mol m^{-2}) considering the vertical NO_3^- diffusive flux (0.2 ± 0.2 mol m^{-2}) as representative of the mixing term. Additional supply through mixing into the surface water during the vegetative season does not appear sufficient to explain the large decoupling (1.6 mol m^{-2}) between NO_3^- uptake and apparent drawdown. Indeed, higher supply requires that both the export and accumulation of organic matter increase (equation (1)), which was not observed. Hence, N recycling within the mixed layer via remineralization and nitrification appears to be a more viable explanation. This perspective is also supported by high daily nitrification rates in the mixed layer (up to ~1 µmol L^{-1} d^{-1}) in November (Figure 4), indicating a tight balance with assimilation rates [*Cavagna et al.*, 2015]. In the next section, we show that the isotopic composition of nitrate also points toward a strong contribution of nitrification to nitrate assimilation over the vegetative season.

3.2. Isotopic Constraints

Analysis of the natural N and O isotopic composition ($\delta^{15}N$ and $\delta^{18}O$) of the various fixed N pools has the potential to yield process rate estimates integrated over seasonal time scales. During NO_3^- assimilation, phytoplankton preferentially incorporate ^{14}N, leaving the residual NO_3^- enriched in ^{15}N [*Sigman et al.*, 1999]. Most field estimates of isotope effects are close to 5–10‰ (i.e., $^{15}\varepsilon$ (‰) = (($^{14}k/^{15}k)^{-1}$) × 1000, where ^{n}k is the rate coefficient for the ^{n}N-containing reactant) [*DiFiore et al.*, 2010]. Since phytoplankton discriminate against ^{15}N and ^{18}O to the same extent ($^{15}\varepsilon \approx {}^{18}\varepsilon$) [*Granger et al.*, 2004, 2010; *Karsh et al.*, 2012], the residual NO_3^- $\delta^{15}N$ and $\delta^{18}O$ rise equally as assimilation proceeds (i.e., coupling between N and O isotopes). In contrast, nitrification decouples N from O isotopes [*Lehmann et al.*, 2004; *Sigman et al.*, 2005]. During NO_3^- assimilation and regeneration, the N isotopes are recycled between the fixed N pools, while the O isotopes are removed by nitrate assimilation (since NO_3^- is reduced to NH_4^+ before assimilation) and then replaced in the nitrification process (NH_4^+ to NO_2^- and then NO_3^-). Nitrified NO_3^- $\delta^{15}N$ will thus depend on the PN $\delta^{15}N$, as well as on the NH_4^+ and NO_2^- branching reactions and associated isotope effects (Figure 5) [*DiFiore et al.*, 2009; *Fripiat et al.*, 2014]. Nitrified NO_3^- $\delta^{18}O$ appears to be close to the $\delta^{18}O$ of the ambient water plus ~1.1‰ [*Casciotti et al.*, 2008; *Sigman et al.*, 2009; *DiFiore et al.*, 2009; *Rafter et al.*, 2013]. Co-culture experiments (combining NH_4^+ oxidizing bacteria, NH_4^+ oxidizing archea, and NO_2^- oxidizing bacteria) give a range for the nitrified NO_3^- $\delta^{18}O$ between −1.5 and 1.3‰ relative to seawater H_2O $\delta^{18}O$ [*Buchwald et al.*, 2012], encompassing field estimates.

At the onset of the spring bloom, NO_3^- $\delta^{15}N$ and $\delta^{18}O$ were relatively constant with depth (Figure 3b). This is in agreement with the relatively small gradient in nitrate concentration and previously low

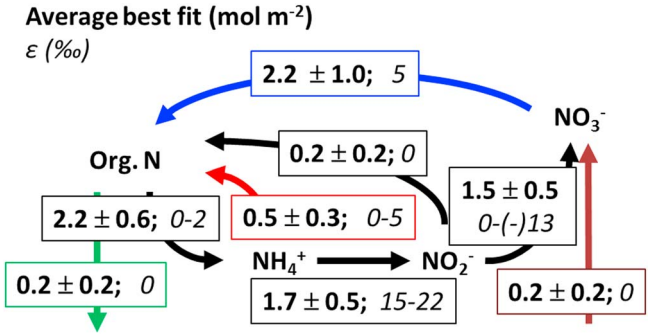

Figure 5. Prescribed and simulated fluxes obtained from the single box nitrogen cycling model (best fit average of 147 simulations ± 1sd). The fluxes (bold numbers) are represented in mol m^{-2} $season^{-1}$. Numbers in italic give the range for the isotope effects (see the auxiliary materials for more detailed discussion). Black arrows are the derived fluxes and colored arrows are the prescribed fluxes (with 90% confidence interval).

biological activity. Associated with the seasonal NO_3^- drawdown, NO_3^- $\delta^{15}N$ and $\delta^{18}O$ increased by 0.9 and 1.5‰, respectively (Figures 2b and 3b). The slopes given by the relationships between Ln($[NO_3^-]$) and NO_3^- $\delta^{15}N$ and $\delta^{18}O$ provide estimates of the net N and O isotope effects associated with NO_3^- consumption (i.e., assuming Rayleigh fractionation, with the assumptions that the reactant and product are neither replenished nor lost from the system) [*Sigman et al.*, 1999]. For the observed NO_3^- depletion, N isotopes (net $^{15}\varepsilon = 3.0 \pm 0.3‰$; $R^2 = 0.80$; P value < 0.001) appeared to be less fractionated than O isotopes (net $^{18}\varepsilon = 4.5 \pm 0.5‰$; $R^2 = 0.71$; P value < 0.001), with both of them lower than summertime field estimates [*DiFiore et al.*, 2010]. Such decoupling between N and O isotopes can also be visualized in terms of the NO_3^- $\delta^{15}N$-$\delta^{18}O$ relationship (relative to the 1:1 reference line, slope = 1; Figure 2d). If NO_3^- assimilation (with $^{15}\varepsilon \approx {}^{18}\varepsilon$) was the only process at work, the isotopic composition should fall on the 1:1 reference line [*Sigman et al.*, 2005]. Instead, mixed layer data from the iron-fertilized plateau show a slope of 1.5 ± 0.1 ($R^2 = 0.87$; P value < 0.001; Figure 2d). Nitrification can explain both this deviation above the 1:1 reference line and the lower net isotope effects compared to summertime field estimates. Nitrification produces NO_3^- with $\delta^{15}N$ decreased more than $\delta^{18}O$ compared to ambient NO_3^- [*Sigman et al.*, 2005, 2009; *Casciotti et al.*, 2008; *DiFiore et al.*, 2009; *Rafter et al.*, 2013].

This important influence of nitrification was further confirmed with the vertical profiles of Δ(15–18) (=NO_3^- $\delta^{15}N$–NO_3^- $\delta^{18}O$) [*Rafter et al.*, 2013]. As for the NO_3^- $\delta^{15}N$-$\delta^{18}O$ relationship, the Δ(15–18) values allow assessment of the decoupling between N and O isotopes. With NO_3^- assimilation as the only process, Δ(15–18) should remain unchanged (=initial Δ(15–18)), since the isotope effects are similar for N and O isotopes. By regenerating NO_3^- with a lower $\delta^{15}N$ than $\delta^{18}O$, nitrification decreases the Δ(15–18) of the initial nitrate pool [*Sigman et al.*, 2005, 2009]. At the onset of the bloom, Δ(15–18) was relatively constant with depth (with a mixed layer Δ(15–18) of 2.5‰; Figure 3b). This initial profile does not show clear evidence of wintertime surface nitrification as suggested with the observed decoupling of N and O isotopes in the upper ocean for the Atlantic sector of the Southern Ocean in winter [*Smart et al.*, 2015]. At the end of the bloom, mixed layer Δ(15–18) had decreased down to ~1.9‰, in agreement with the occurrence of spring-summer mixed layer nitrification (early spring Δ(15–18) minus late summer Δ(15–18) = 0.5 ± 0.3‰). Since here we report $NO_3^- + NO_2^-$ $\delta^{15}N$ and $\delta^{18}O$, an interference from the nitrite pool would also have the potential to affect differently N and O isotopes, implying possibly that an effect of nitrification is not required to explain the observations [*Smart et al.*, 2015; *Fawcett et al.*, 2015; see supporting information for a detailed description of this interference]. However, since (i) we are looking at the seasonal changes in both $\delta^{15}N$ and $\delta^{18}O$ (i.e., seasonal decoupling between N and O isotopes) and (ii) there is no significant change in the contribution of NO_2^- into the $NO_3^- + NO_2^-$ pool (1.2 ± 0.5 %) between spring and summer, an interference from an invariant NO_2^- $\delta^{15}N$ and $\delta^{18}O$ will have no effect on our assessment of the decoupling between N and O isotopes (i.e., early spring Δ(15–18) minus late summer Δ(15–18) = 0.5‰). It is only in case NO_2^- $\delta^{15}N$ and $\delta^{18}O$ vary significantly between spring and summer that a bias could occur. By taking the range for both NO_2^- $\delta^{15}N$ and $\delta^{18}O$ that we can expect (including the methodological bias for O isotopes), the seasonal decoupling between N and O isotopes is 0.56 ± 0.22‰. Such a range is indistinguishable from the precision given on the observations (0.53 ± 0.30‰), implying a negligible impact of nitrite interference on the observed seasonal decoupling between N and O isotopes in the mixed layer.

A distinct subsurface (150 m) Δ(15–18) minimum was also observed in late summer (Figure 3b), coinciding with the subsurface NH_4^+ and chl *a* maxima [*Mosseri et al.*, 2008]. Remineralization, coupled with nitrification,

of this accumulated biomass is a likely explanation for this distinct Δ(15–18) minimum (further discussed below). One could argue that such low-Δ(15–18) subsurface NO_3^- can be supplied into the mixed layer by vertical mixing in summer, and thus that mixed layer nitrification would not be necessary to explain the observed decoupling between N and O isotopes in the mixed layer.

In the following two sections, we use the vertically resolved version of the model and the water column profiles of the nitrate N and O isotopes to address the vertical distribution of nitrification (section 3.3) and to obtain optimized quantitative estimates of the contribution of nitrification to NO_3^- assimilation in the mixed layer (using the single box model; section 3.4).

3.3. Surface Versus Subsurface Nitrification

The southeast Kerguelen plateau is characterized by high-vertical-eddy diffusivities [*Park et al*., 2008b, 2014] and a deep mixed layer (100 ± 40 m; average ± sd of 56 CTD profiles during KEOPS 1 and 2). The euphotic layer (100 to 1% of photosynthetically active radiation) is more shallow, 53 ± 16 m (average ± sd of 21 profiles during KEOPS 1 and 2). Until recently, nitrification was thought to be inhibited by light. However, effective measurements of nitrification rate show a maximum near the bottom of the euphotic zone (5–10% PAR) [*Ward*, 2007], i.e., within the mixed layer for the Kerguelen Plateau. A decoupling with depth between NO_3^- assimilation (light dependent) and nitrification (partly light inhibited) may occur either within the mixed layer, implying that recently nitrified NO_3^- is directly available for subsequent phytoplankton assimilation (case a) or only below the mixed layer in the extreme case of light inhibition (case b). In the latter scenario, recently nitrified NO_3^- must be supplied into the summer mixed layer through vertical mixing.

To determine which of these scenarios prevailed above the Kerguelen Plateau, we developed a multibox vertically resolved (0–250 m) model to qualitatively describe the seasonal evolution of NO_3^- $\delta^{15}N$ and $\delta^{18}O$ from the onset (October) to the collapse (February) of the bloom (see the supporting information for a detailed model description and sensitivity analysis). Briefly there are three processes presenting a contrasting vertical distribution (Figure S2 in the supporting information): (i) vertical mixing between adjacent layers, (ii) NO_3^- assimilation in the mixed layer, and (iii) nitrification, either considered to represent a fraction of NO_3^- assimilation in the mixed layer (mixed layer nitrification) or to decrease with depth from a subsurface maximum at the base of the mixed layer (subsurface nitrification) following particulate organic N attenuation with depth [*Berelson*, 2001]. In the model, nitrification produces NO_3^- with $\delta^{15}N$ of 1.9‰ and $\delta^{18}O$ of 0.6‰, reflecting the average PN $\delta^{15}N$ and H_2O $\delta^{18}O$ (−0.5‰ + 1.1‰), respectively [*Archambeau et al*., 1998; *Casciotti et al*., 2008; *Sigman et al*., 2009; *Rafter et al*., 2013].

The model satisfactorily reproduces the NO_3^- concentration, $\delta^{15}N$, and $\delta^{18}O$ profiles (Figures 3a and 3b). The model simulations reveal contrasting vertical Δ(15–18) distributions (= NO_3^- $\delta^{15}N$ – NO_3^- $\delta^{18}O$), depending on the nitrification scenario (Figures 3b and 6). For the case of nitrification occurring only below the mixed layer, the lowest simulated Δ(15–18) values (2.3‰; Figures 3b and 6b) are found below the mixed layer where nitrification is strongest. Vertical mixing propagates this anomaly both upward and downward. For the case of nitrification in both the mixed layer and the subsurface, simulated Δ(15–18) values decrease upward (down to 1.9‰; Figures 3b and 6a).

In general, the observed Δ(15–18) values for the iron-fertilized plateau are consistent with the modeled occurrence of nitrification in both surface and subsurface waters (Figure 6). The model cannot reproduce the observed low Δ(15–18) values in the mixed layer without allowing for significant surface nitrification.

However, the model cannot also reproduce the distinct subsurface (150 m) Δ(15–18) minimum in late summer. In order to do so, recently nitrified NO_3^- should bear a $\delta^{18}O$ above ~7‰ or a $\delta^{15}N$ below ~−3‰ or a combination of both (Figure 6c). Such high values for recently nitrified NO_3^- $\delta^{18}O$ are well above reported values [*Sigman et al*., 2009; *Buchwald et al*., 2012], except for one outlier at 5.3‰ in *Buchwald et al*. [2012]. One of the main factors driving variations in the recently nitrified NO_3^- $\delta^{18}O$ is the nitrite residence time, setting the degree of exchange between the O atoms in H_2O and NO_2^- [*Buchwald et al*., 2012]. Exchanges lead to higher NO_3^- $\delta^{18}O$ because of the equilibrium isotope effect between NO_2^- and H_2O [*Casciotti et al*., 2007; *Buchwald et al*., 2012]. It is likely that the higher residence time for nitrite in the deep Chl *a* maximum (either via NO_2^- production rates in excess of NO_2^- consumption rates and/or slower overall rates) is the cause for the subsurface Δ(15–18) minimum. Alternatively, lower recently nitrified NO_3^- $\delta^{15}N$ can be achieved with an

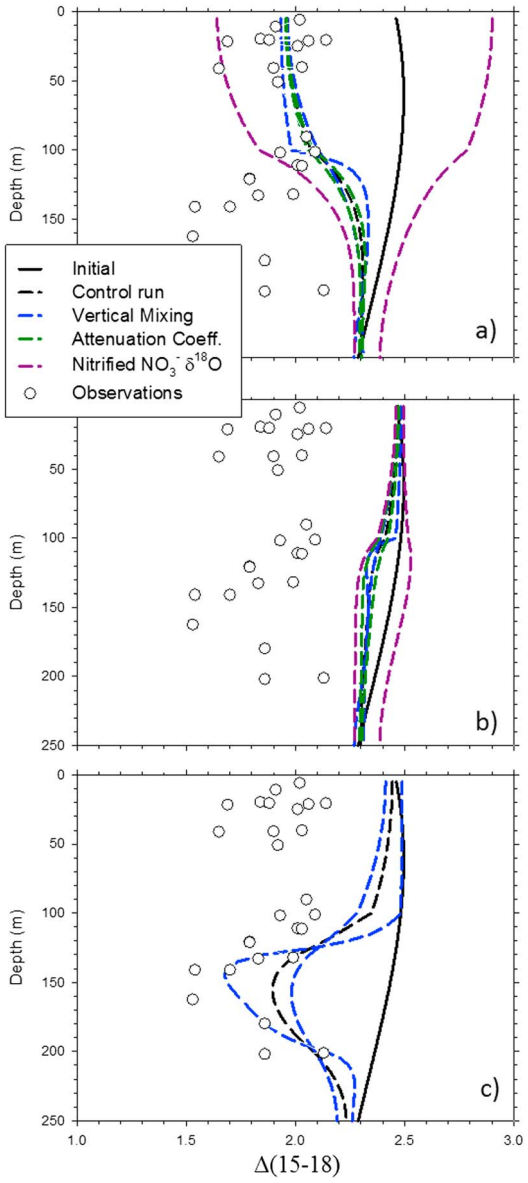

Figure 6. Sensitivity of the time-dependent one-dimensional vertical box model (0–250 m, 50 layers) to (i) the depth attenuation coefficient for the export of organic matter (green dashed line; $b = 0.6–1.3$, i.e., the oceanic range) [*Berelson*, 2001]; (ii) to the vertical mixing rates (blue dashed lines; with a net upward nitrate supply varying from 0.03 to 0.3 mol m^{-2}, implying a large range in the upward and downward fluxes due to a small vertical nitrate gradient; see supporting information for a detailed description on the model sensitivity); and (iii) to the newly produced NO_3^- $\delta^{18}O$ (purple dashed lines, −1.5 to 1.3‰) [*Buchwald et al.*, 2012]. The initial conditions are represented by the black line (A3-1 KEOPS2 station; 20 October). The dashed black line is the control run ($b = 0.82$; newly produced nitrate $\delta^{18}O = 0.6$‰; net nitrate supply into the mixed layer = 0.2 mol m^{-2}). The final conditions are represented by the empty circles (KEOPS 1 station; January–February). (a) One-dimensional vertical box model with nitrification in both surface and subsurface. (b) One-dimensional vertical box model with nitrification in subsurface only. (c) One-dimensional vertical box model with no nitrification above 125 m (only at 125 m and attenuated with depth below, corresponding to the subsurface chl *a* maximum) and a value for newly produced nitrate $\delta^{18}O$ at 7‰ between 125 and 200 m.

imbalance between NH_4^+ production and consumption processes, as expected from the strong NH_4^+ accumulation (2.3 μmol l^{-1}) at the deep Chl *a* maximum. This imbalance allows the expression of the isotope effect associated with NH_4^+ oxidation (15–22‰), leading to the production of low-$\delta^{15}N$ nitrate [*Casciotti et al.*, 2003; *Santoro and Casciotti*, 2011].

However, even with these extreme values for recently nitrified NO_3^- $\delta^{15}N$ and $\delta^{18}O$ in the subsurface and a large tested range for the vertical mixing rates, surface nitrification is still required in order to reproduce the low-Δ(15–18) values in the mixed layer (Figure 6c; see supporting information for a more detailed description of the model sensitivity). As noted earlier, this result is also in agreement with daily nitrification rates (up to ~1 μmol L^{-1} d^{-1}) in the mixed layer at the peak of the bloom (Figure 4) [*Cavagna et al.*, 2015].

3.4. Surface Contribution of Nitrification to NO_3^- Assimilation

It is generally assumed that NO_3^- in the Southern Ocean is mainly assimilated in summer and replenished by vertical mixing during the winter months. Low nitrification rates in the mixed layer have been indeed reported in the HNLC areas (<0.1 μmol L^{-1} d^{-1}) but only for fall and winter when primary production and remineralization are expected to be low [*Olson*, 1981; *Bianchi et al.*, 1997]. In contrast, in spring (November), daily nitrification rates in the mixed layer were much higher (up to ~1 μmol L^{-1} d^{-1}) over the southeast Kerguelen Plateau (Figure 4) [*Cavagna et al.*, 2015].

To further constrain the seasonal contribution of nitrification to NO_3^- assimilation, we used a time-dependent single-box model for the mixed layer (see supporting information for a more detailed description of the model). The model simulates the change in concentration of the fixed N pools (PN, NH_4^+, NO_2^-, and NO_3^-) and their isotopic compositions ($\delta^{15}N$ for all of them and $\delta^{18}O$ for NO_3^-) in the time frame given by the

observations (from October to February). During NO_3^- assimilation and regeneration, N isotopes are recycled between the fixed N pools (Figure 5), while O isotopes are removed, and then replaced by the nitrification process [*Sigman et al.*, 2005]. We assume that recently nitrified NO_3^- has a $\delta^{18}O$ value equal to that of ambient seawater plus 1.1‰ [*Casciotti et al.*, 2008; *Sigman et al.*, 2009; *Rafter et al.*, 2013].

As previously described in the methods section, some N fluxes were independently estimated from observations and therefore prescribed (colored arrows in Figure 5). Both ammonium (NH_4^+) and nitrite (NO_2^-) concentrations in the mixed layer remained relatively low (Figure 2a), indicating a close balance between their production and consumption processes. This left us with two unknowns, both related to the relative contribution of the processes associated with the NH_4^+ and NO_2^- removals, i.e., assimilation and oxidation (branching reactions, black arrows in Figure 5).

We solve the model differential equations by varying both NH_4^+ assimilation/ammonification and NO_2^- assimilation/NH_4^+ oxidation ratios, targeting the best agreement between the observations (and their uncertainties) at the collapse of the bloom (KEOPS 1) and the model counterparts. To measure this agreement, we use the minimum cost function, searching for the lowest standardized residual [*Elskens et al.*, 2007] (see supporting information for a more detailed description of the optimization scheme and the model sensitivity). By varying both NH_4^+ assimilation/ammonification and NO_2^- assimilation/NH_4^+ oxidation ratios, the best fits (within the error range of the observations; Figures 2a and 2b) impose a contribution of nitrification to NO_3^- assimilation between 40 and 80%. The model is highly sensitive to the NO_3^- uptake term, with a contribution of nitrification in the lower range at lower rates. The comparison between the best fit model curves for NO_3^- uptake and satellite Chl *a* observation (Figure 2c) may suggest that it is likely that the NO_3^- uptake term might be in the lower range of the estimations. Such a contribution for nitrification fits the upper oceanic range reported in the literature [*Ward*, 2007; *Yool et al.*, 2007] and implies that NO_3^- is strongly recycled in the mixed layer over the Kerguelen Plateau. This analysis does not include DON, for which measurements were only reported for October–November and exceeded by up to 4 $\mu mol\,L^{-1}$ the concentration in the HNLC area [*Ogawa et al.*, 1999; *Blain et al.*, 2015]. Field and laboratory studies indicate that both bacteria and zooplankton preferentially degrade low-$\delta^{15}N$ organic N to ammonium, with a net isotope effect of ~2–3‰ [*Checkley and Miller*, 1989; *Knapp et al.*, 2011; *Möbius*, 2013, and references therein]. With the reasonable assumption that this fractionation is identical for ammonification of PN and DON (PN, DON → NH_4^+) and that the DON release (PN → DON) has little or no fractionation [*Knapp et al.*, 2011, and references therein], recently produced DON $\delta^{15}N$ will be close to PN $\delta^{15}N$ [*Fripiat et al.*, 2015]. Adding this 4 $\mu mol\,L^{-1}$ of DON to the final PN pool, assuming that it is an actively cycling N pool [*Bronk et al.*, 1994], allows us to improve the fit between the measured and simulated concentrations (Figures 2a and 2b) without changing the contribution of nitrification to NO_3^- assimilation (0.66 ± 0.09 and 0.72 ± 0.08, average ± sd, without and with the DON, respectively; $n = 147$ simulations).

We acknowledge that an uncertainty remains on the parameterization of the mixing term (set to 0.2 ± 0.2 $mol\,m^{-2}\,yr^{-1}$ from the vertical diffusivity constant and vertical nitrate gradient; Figure 5). If the nitrate supply was revised upward (e.g., to reflect other processes such as entrainment by episodic mixed layer deepening), this mechanism would supply low Δ(15–18) nitrate into the mixed layer (from the subsurface nitrate Δ(15–18) minimum; Figure 3b) and imply an overall lower contribution of surface nitrification to nitrate assimilation. However, the relatively good fit between the seasonal (i.e., single box model) and daily (i.e., ^{15}N incubations) estimates argues against this possibility. In addition, in simulations with increased vertical nitrate supply (see Figure S5 in the supporting information), the model cannot reproduce the observations (in the limit of their uncertainties) for a nitrate supply higher than 0.6–0.8 $mol\,m^{-2}\,yr^{-1}$, and the ratio of nitrification to nitrate assimilation is still ~0.5. We close this discussion of resupply by noting that while our assessment has been one-dimensional, estimated horizontal resupply from surrounding HNLC waters is insufficient [~30% of seasonal depletion; *Jouandet et al.*, 2008] to change our conclusions.

The optimal estimated integrated nitrification in the mixed layer over the vegetative season is 1.5 ± 0.5 $mol\,m^{-2}$ (Figure 5), with a mixed layer average of 0.13 ± 0.07 $\mu mol\,L^{-1}\,d^{-1}$ (117 days and a mixed layer depth of 100 ± 40 m). In comparison, rates in other open ocean systems range from a few to a few hundred nanomolar per day [*Ward*, 2007] with the highest rates reaching 0.75 $\mu mol\,L^{-1}\,d^{-1}$ in the Peru upwelling [*Lipschultz et al.*, 1991].

3.5. Mechanistic Understanding and Biogeochemical Implications

The observed decoupling between mixed layer depth (MLD) and euphotic layer depth (Z_{eu}) can explain why the productive Kerguelen Plateau appears to be a favorable environment for nitrification to contribute significantly to nitrate assimilation in the surface water. The spring mixed layer for this area extends deeply into the water column (100 ± 40 m), well below the euphotic zone depth (53 ± 16 m). Productive areas are known to present high light attenuation with depth [*Kirk*, 1992]. This allows NO_3^- to be assimilated in the upper parts of the mixed layer, where light is sufficient to sustain high primary production and regenerated in the lower parts, where light is insufficient to inhibit nitrification [*Ward*, 2007]. Nitrate assimilation and regeneration can thus take place within the same water mass (i.e., mixed layer). The vertical profile indeed shows that NO_3^- assimilation rates decrease with depth, and nitrification rates increase with depth, within the mixed layer (Figure 4) [*Cavagna et al*., 2015]. At the bottom and below the euphotic layer, light intensity is severely reduced, phytoplankton are light limited, and nitrifiers can compete with phytoplankton for the ammonium produced by remineralization [*Ward*, 2007; *Martens-Habbena et al*., 2009; *Newell et al*., 2011; *Smith et al*., 2014]. Iron fertilization leads to overall higher primary productivity [*Cavagna et al*., 2015] and likely yields more ammonium from remineralization for nitrification. Several studies have shown that the microbial food web and grazing were indeed stimulated over the southeast Kerguelen Plateau [*Brussaard et al*., 2008; *Carlotti et al*., 2008; *Sarthou et al*., 2008; *Christaki et al*., 2015; *Malits et al*., 2014]. The absolute rate of nitrification likely tracks the overall productivity of the Kerguelen Plateau system (estimated to be 196 g C m^{-2} yr^{-1} by integrating the net primary production curve in Figure 2), which is in the upper portion of the global oceanic range [*Behrenfeld and Falkowski*, 1997; *Cavagna et al*., 2015]. To summarize, the balance between nitrate assimilation and nitrification in the mixed layer is likely driven by the decoupling between MLD and Z_{eu}, and the absolute rates of both nitrification and N assimilation are dependent on the overall productivity.

To see if such decoupling is common in the Southern Ocean, we looked at MLD from Argo profiles, mainly between 2004 and 2006 [*Dong et al*., 2008] and Z_{eu} from satellite Chl *a* distributions for October 2004 to February 2005 (available at http://hermes.acri.fr/index.php) [*Morel et al*., 2007]. We focused on the open (i.e., ice free) Antarctic zone (OAZ) [*DiFiore et al*., 2009] between the Antarctic Polar Front and Southern Antarctic Circumpolar Current Front, which is representative of the water masses over the southeast Kerguelen Plateau [*Park et al*., 2008a, 2008b]. MLD is commonly deeper than Z_{eu} in October and November (Figure 7; Mann-Whitney rank sum test, P value < 0.001). The opposite is true from December to February (Mann-Whitney rank sum test, P value < 0.05). In the pelagic area south of 50°S, the bloom starts in October, peaks at the end of November–December, and collapses in January–February [*Arrigo et al*., 2008]. During a significant fraction of time (approximately from the onset to the peak of the bloom), MLD is therefore commonly deeper than Z_{eu}. This analysis suggests that the observed close balance between nitrate assimilation and nitrification may be a more general characteristic of the open Antarctic zone in early spring than previously thought. This needs to be further confirmed with spatially distributed studies, as well as direct nitrification measurements, which are still lacking in both spring and summer in this area [*Olson*, 1981; *Bianchi et al*., 1997]. The overall seasonal effect may not be as strong in the OAZ as over the southeast Kerguelen Plateau. Over the plateau, summer MLD tends to be deeper than in the OAZ (Mann-Whitney rank sum test, P value < 0.001, with a median estimate up to ~25 m deeper) and Z_{eu} to be shallower owing to higher productivity (down to ~35–40 m at the peak of the bloom; Figure 4). The decoupling (MLD $> Z_{eu}$) is therefore maintained for a longer period of time (especially in December; Figure 7), likely allowing a higher contribution of nitrification to nitrate assimilation for this specific area. However, this study adds to the growing body of work (wintertime Antarctic zone and Antarctic sea ice, both low-light environments) [*Fripiat et al*., 2014, 2015; *Smart et al*., 2015] that suggest also surface nitrification in the Southern Ocean is more important than previously thought.

It is generally considered that the discrimination of nitrate and ammonium uptake enables resolving new from regenerated production [*Dudgale and Goering*, 1967], i.e., primary production sustained by nitrate from primary production sustained by NH_4^+. This paradigm assumes, among other things, that nitrate is mainly supplied to the euphotic layer through vertical mixing from the ocean interior. At steady state the upward flux of nitrate must balance the downward flux of sinking PN, i.e., new primary production [*Eppley and Peterson*, 1979]. In this paradigm, nitrification occurs below the euphotic layer. In most of the ocean (e.g. low-latitude areas) Z_{eu} is deeper than MLD, implying that regenerated nitrate is not directly available to

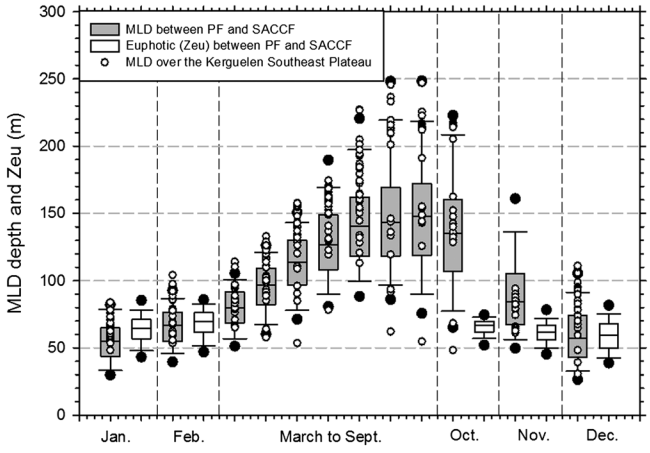

Figure 7. Mixed layer depth (gray boxes) and euphotic layer depth (white boxes) distributions in the open Antarctic zone (from the monthly climatology given in *Dong et al*. [2008] and available at http://hermes.acri.fr/index.php). MLD over the southeast Kerguelen Plateau is represented by the white dots (also from the climatology given in *Dong et al*. [2008] for the isobaths of ~500 m). MLD was computed from individual Argo profiles based on the threshold method with a finite-density difference criterion (0.03 kg m^{-3}) from a near-surface reference value. The MLD climatology was mapped onto a 1°×1° grid [*Dong et al*., 2008]. Euphotic depth (1% PAR) was derived from Sea-wiewing Wide Field-of-view Sensor products of surface Chl *a* (following *Morel et al*. [2007]. The Z_{eu} climatology represents the binned monthly values mapped onto a 100 km × 100 km grid. The locations of the fronts given in *Orsi et al*. [1995] have been used to retrieve the data corresponding to the open Antarctic zone (between the Antarctic Polar Front and Southern Antarctic Circumpolar Current Front). The boxes, whiskers, and symbols cover the 25th to 75th, the 10th to 90th, and the 5th to 95th percentiles, respectively.

phytoplankton, in agreement with the approach described by *Dudgale and Goering* [1967] to assess new primary production. The particularity of the Kerguelen Plateau, and the open Antarctic zone in spring, is that the MLD is commonly deeper than Z_{eu}, allowing the nitrate produced by nitrification to be easily transported into the euphotic, thereby directly supporting regenerated primary production. The new production paradigm in the sense of *Dudgale and Goering* [1967] has been recently challenged with the observations of significant nitrification in the euphotic layer, even in the low-latitude ocean [*Yool et al*., 2007]. Their modeling study suggests that nitrification could account for about half of the nitrate consumed in the euphotic layer by phytoplankton at the global scale. However, the Southern Ocean was still considered to obey the initial paradigm with presumed low nitrification rates [*Olson*, 1981; *Bianchi et al*., 1997; *Yool et al*., 2007; *DiFiore et al*., 2009]. A commonly used metric to assess new primary production is the *f* ratio (i.e., NO_3^- uptake/[NO_3^- uptake + NH_4^+ uptake]). If one knows primary productivity, new primary production can be estimated by multiplying it by the *f* ratio [*Dudgale and Goering*, 1967]. The *f* ratio over the southeast Kerguelen Plateau in spring is in the range of 0.75–0.85 [*Cavagna et al*., 2015; *Trull et al*., 2015]. By considering the fraction of NO_3^- assimilation provided through nitrification, the corrected *f* ratio decreases to 0.26. This value is similar to the average PN export efficiency over the southeast Kerguelen Plateau, 0.02–0.30 (i.e., the fraction of primary production that is exported from the upper 100 m) as determined from the ^{234}Th deficit and the ^{234}Th:N ratio of the exported organic matter [*Savoye et al*., 2008; *Planchon et al*., 2015]. Nitrate-based primary production in this iron-fertilized bloom appears mainly to return to nitrate through nitrification. Overall, the concomitant high residual NO_3^- concentration (>20 μmol L^{-1}) at the end of the vegetative season emphasizes that the lack of iron is not the only driver of the high-nutrient low-chlorophyll character in the Antarctic zone. This study highlights the role of low light level in deep mixed layers, already recognized as a co-limitation factor, together with iron, for primary production [*Martin et al*., 1990; *Mitchel et al*., 1991; *de Baar et al*., 2005], via its impact on nitrification and the regeneration of nitrate within the mixed layer.

Finally, we consider the possibility that high nitrification provides a feedback to climate warming via N_2O production that counters the removal of CO_2 by the iron-enhanced biological pump. *Fuhrman and Capone* [1991] hypothesized that iron fertilization by leading to higher primary productivity should promote the formation of nitrous oxide (N_2O) via stimulation of the overall N cycle (assimilation + regeneration). This was not observed. There were no indications of significant N_2O production in the mixed layer over the southeast Kerguelen Plateau at the onset of the bloom [*Farias et al*., 2015], with estimated atmosphere-ocean N_2O fluxes ranging from −10.5 to 5.1 μmol m^{-2} d^{-1} (with positive values representing fluxes from the ocean to the atmosphere). Nitrification is thought to dominate N_2O production in oxic water columns [*Bange*, 2007]. N_2O is a by-product of nitrification with a N_2O yield (moles of N_2O produced per mole ammonium consumed × 100)

ranging between 0.001 and 10% [*Goreau et al.*, 1980; *Yoshiba et al.*, 1989; *Bange*, 2007; *Frame and Casciotti*, 2010; *Löscher et al.*, 2012]. In the conditions encountered in the summer mixed layer over the southeast Kerguelen Plateau (oxic conditions and low-nitrite concentrations), the N_2O yield should be in the lower range (0.001 to 0.05%) [*Frame and Casciotti*, 2010; *Löscher et al.*, 2012]. By taking this range and the average daily nitrification rates of 12.8 mmol m^{-2} d^{-1} (from the single box model), N_2O production by nitrification should range between 0.1 and 6.4 μmol m^{-2} d^{-1}, encompassing the observed range for the atmosphere-ocean N_2O fluxes [*Farias et al.*, 2015]. Thus, the enhanced surface nitrification does not seem to increase significantly N_2O production in this specific iron-fertilized area with therefore no significant effect on climate. This in agreement with the study of *Clark et al.* [2014] in the North Sea showing nitrous oxide concentration in the mixed layer comparable to that of the atmosphere in spite of a close balance between assimilation and regeneration (i.e., nitrification) processes for the dissolved inorganic N forms (NH_4^+, NO_2^-, and NO_3^-).

4. Conclusion

Although iron fertilization clearly stimulates primary productivity and total nitrogen uptake over the southeast Kerguelen Plateau [*Cavagna et al.*, 2015], nitrate concentration at the end of the growing period is only slightly lower than the levels encountered in surrounding high-nutrient low-chlorophyll waters [*Pondaven et al.*, 2000; *Nelson et al.*, 2002; *Blain et al.*, 2007]. We suggest that this condition arises because mixed layer nitrification is significant over the Kerguelen Plateau and is sufficient to sustain most of the NO_3^- assimilation on a seasonal basis (40 to 80 %). The large contribution of nitrification is inferred from the imbalance between nitrate assimilation (from nitrate uptake rates) and apparent nitrate depletion, implying another source of nitrate, and the decoupling between N and O isotopes in upper oceanic nitrate, fingerprinting the occurrence of nitrification. This is further confirmed by high daily nitrification rates measured in incubations in November [*Cavagna et al.*, 2015]. The large decoupling between the euphotic layer and mixed layer depths (with MLD $> Z_{eu}$) appears to be the environmental condition that allows nitrifiers to so successfully compete with phytoplankton for the reprocessing of ammonium. We encourage further investigations on the significance of nitrification in the Southern Ocean. Previous studies reporting nitrification rates have been mainly performed during unproductive seasons [*Olson*, 1981; *Bianchi et al.*, 1997]. It is likely that a prevailing deep mixed layer in this ocean imposes a tighter coupling between nitrate consuming and regenerating processes than previously expected, especially in early spring. Together with the recent studies of *Smart et al.* [2015] and *Fripiat et al.* [2014, 2015] in wintertime Antarctic zone and in sea ice (both low-light environments), this study shows that there is a growing recognition of the importance of nitrification at the surface of the Southern Ocean.

Acknowledgments

Data are available as in the data repositories of both KEOPS 1 (http://www.obs-vlfr.fr/proof/vt/op/ec/keops/keo.htm) and KEOPS 2 (http://www.obs-vlfr.fr/proof/php/keops2/x_datalist_1.php?xxop=keops2&xxcamp=keops2). We thank the Captain and the crew of *Marion-Dufresne* as well as KEOPS 1 and 2 chief scientists B. Quéguiner and S. Blain for their assistance and help during the cruises. We are grateful to the Institut Paul Emile Victor for having granted us access to the *Marion-Dufresne*. The research was conducted with grants from (Belgian Science Policy, grant SD/CA/05A), Flanders Research Foundation (FWO; grant G071512N); Vrije Universiteit Brussel (Strategic Research Plan); and the Antarctic Climate and Ecosystem Cooperative Research Center. F. Fripiat is currently a postdoctoral fellow at FWO, Flanders Research Foundation. The interpretation of the data was greatly aided by expertise F. Fripiat learned during his time in the Sigman laboratory at Princeton University.

References

Archambeau, A.-S., C. Pierre, A. Poisson, and B. Schauer (1998), Distributions of oxygen and carbon stable isotope and CFC-12 in the water masses of the Southern Ocean at 30°E from South Africa to Antarctica: Results of the CIVA1 cruise, *J. Mar. Syst.*, *17*, 25–38.

Arrigo, K. R., G. L. van Dijken, and S. Bushinsky (2008), Primary production in the Southern Ocean, 1997–2006, *J. Geophys. Res.*, *113*, C08004, doi:10.1029/2007JC004551.

Bange, H. W. (2007), Gaseous nitrogen compounds (NO, N_2O, N_2, NH_3) in the ocean, in *Nitrogen in the Marine Environment*, edited by D. G. Capone et al., Elsevier, Amsterdam, Netherlands.

Behrenfeld, M. J., and P. G. Falkowski (1997), Photosynthetic rates derived from satellite-based chlorophyll concentration, *Limnol. Oceanogr.*, *42*(1), 1–20.

Berelson, W. M. (2001), The flux of particulate organic carbon into the ocean interior: A comparison of four U.S. JGOFS, Regional Studies, *Oceanography*, *14*, 59–67.

Bianchi, M., F. Feliatra, P. Tréguer, M.-A. Vincendeau, and J. Morvan (1997), Nitrification rates, ammonium and nitrate distribution in upper layers of the water column and in sediments of the Indian sector of the Southern Ocean, *Deep Sea Res., Part II*, *44*(5), 1017–1032.

Blain, S., et al. (2007), Effect of natural iron fertilization on carbon sequestration in the Southern Ocean, *Nature*, *446*, 1070–1074, doi:10.1038/nature05700.

Blain, S., J. Capparos, A. Guéneuguès, I. Obernosterer, and L. Oriol (2015), Distributions and stoichiometry of dissolved nitrogen and phosphorus in the iron fertilized region near Kerguelen (Southern Ocean), *Biogeosciences*, *12*, 623–635.

Böhlke, J. K., S. J. Mroczkowski, and T. B. Coplen (2003), Oxygen isotope in nitrate: new reference materials for ^{18}O:^{17}O:^{16}O measurements and observations on nitrate-water equilibration, *Rapid Commun. Mass Spectrom.*, *17*, 1835–1846.

Bronk, D. A., P. M. Glibert, and B. B. Ward (1994), Nitrogen uptake, dissolved organic nitrogen release, and new production, *Science*, *265*, 1843–1846.

Brussaard, C. P. D., K. R. Timmermans, J. Uitz, and M. J. W. Veldhuis (2008), Virioplankton dynamics and virally induced phytoplankton lysis versus microzooplankton grazing southeast of the Kerguelen (Southern Ocean), *Deep Sea Res., Part II*, *55*, 752–765.

Buchwald, C., A. E. Santoro, M. R. McIlvin, and K. L. Casciotti (2012), Oxygen isotopic composition of nitrate and nitrite produced by nitrifying Cocultures and natural marine assemblages, *Limnol. Oceanogr.*, *57*(5), 1361–1375.

Buesseler, K. O., et al. (2006), An assessment of particulate organic carbon to thorium-234 ratios in the ocean and their impact on the application of ^{234}Th as a POC flux proxy, *Mar. Chem.*, *100*, 213–233.

Carlotti, F., D. Thibault-Botha, A. Nowaczyk, and D. Lefèvre (2008), Zooplankton community structure, biomass, and role in carbon fluxes during the second half of a phytoplankton bloom in the eastern sector of the Kerguelen Shelf (January-February 2005), *Deep Sea Res., Part II*, *55*, 720–733.

Casciotti, K. L., D. M. Sigman, M. Galanter Hastings, J. K. Böhlke, and A. Hilkert (2002), A measurement of the oxygen isotopic composition of nitrate in seawater and freshwater using the denitrifier method, *Anal. Chem.*, *74*, 4905–4912.

Casciotti, K. L., D. M. Sigman, and B. B. Ward (2003), Linking diversity and stable isotope fractionation in ammonia-oxidizing bacteria, *Geomicrobiol. J.*, *20*, 335–353.

Casciotti, K. L., J. K. Böhlke, M. R. McIlvin, S. J. Mroczkwski, and J. E. Hannon (2007), Oxygen isotopes in nitrite: Analysis, calibration, and equilibration, *Anal. Chem.*, *79*, 2427–2436, doi:10.1021/ac061598h.

Casciotti, K. L., T. W. Trull, D. M. Glover, and D. Davies (2008), Constraints on nitrogen cycling at the subtropical North Pacific Station ALOHA from isotopic measurements of nitrate and particulate nitrogen, *Deep Sea Res., Part II*, *55*, 1661–1672.

Cavagna, A.-J., et al. (2015), Biological productivity regime and associated N cycling in the surface waters over and downstream the Kerguelen Island area, Southern Ocean, *Biogeosci. Discuss.*, *11*, 18,073–18,104, doi:10.5194/bgd-11-18073-2014.

Checkley, D. M., and C. A. Miller (1989), Nitrogen isotope fractionation by oceanic zooplankton, *Deep Sea Res.*, *36*(10), 1449–1456.

Christaki, U., D. Lefèvre, C. Georges, J. Colombet, P. Catala, C. Courties, T. Sime-Ngando, S. Blain, and I. Obernosterer (2015), Microbial food web dynamics during spring phytoplankton blooms in the naturally iron-fertilized Kerguelen area (Southern Ocean), *Biogeosciences*, *11*, 6739–6753.

Clark, D. R., I. J. Brown, A. P. Rees, P. J. Somerfield, and P. I. Miller (2014), The influence of ocean acidification on nitrogen regeneration and nitrous oxide production in the northwest European shelf sea, *Biogeosciences*, *11*, 4985–5005.

de Baar, H. J. W., et al. (2005), Synthesis of iron fertilization experiments: From the Iron Age in the Age of enlightenment, *J. Geophys. Res.*, *110*, C09S16, doi:10.1029/2004JC002601.

Dehairs, F., et al. (2015), Nitrogen cycling in the Southern Ocean Kerguelen plateau area: Evidence for significant surface nitrification from nitrate isotopic compositions, *Biogeosciences*, *12*, 1459–1482.

DiFiore, P. J., D. M. Sigman, and R. B. Dunbar (2009), Upper ocean nitrogen fluxes in the Polar Antarctic Zone: Constraints from the oxygen and nitrogen isotopes of nitrate, *Geochem. Geophys. Geosyst.*, *10*, Q11016, doi:10.1029/2009GC002468.

Difiore, P. J., D. M. Sigman, K. L. Karsh, T. W. Trull, R. B. Dunbar, and R. S. Robinson (2010), Poleward decrease in the isotope effect of nitrate assimilation across the Southern Ocean, *Geophys. Res. Lett.*, *37*, L17601, doi:10.1029/2010GL044090.

Dong, S., J. Sprintall, S. T. Gille, and L. Talley (2008), Southern Ocean mixed-layer depth from Argo float profiles, *J. Geophys. Res.*, *113*, C06013, doi:10.1029/2006JC004051.

Dudgale, R. C., and J. J. Goering (1967), Uptake of new and regenerated forms of nitrogen in primary production, *Limnol. Oceanogr.*, *12*, 196–206.

Elskens, M., A. de Brauwere, C. Beucher, R. Corvaisier, N. Savoye, P. Tréguer, and W. Baeyens (2007), Statistical process control in assessing production and dissolution rates of biogenic silica in marine environments, *Mar. Chem.*, *106*, 272–286.

Eppley, R. W., and B. J. Peterson (1979), Particulate organic matter flux and planktonic new production in the deep ocean, *Nature*, *282*, 677–680.

Farias, L., L. Florez-Leiva, V. Besoain, G. Sarthou, and C. Fernandez (2015), Dissolved greenhouse gases (nitrous oxide and methane) associated with the naturally iron-fertilized Kerguelen region (KEOPS2 cruise) in the Southern Ocean, *Biogeosciences*, *12*, 1925–1940.

Fawcett, S. E., B. B. Ward, M. W. Lomas, and D. M. Sigman (2015), Vertical decoupling of nitrate assimilation and nitrification in the Sargasso Sea, *Deep Sea Res., Part I*, *103*, 64–72.

Frame, C. H., and K. L. Casciotti (2010), Biogeochemical controls and isotopic signatures of nitrous oxide production by a marine ammonia-oxidizing bacterium, *Biogeosciences*, *7*, 2695–2709.

Fripiat, F., D. M. Sigman, S. E. Fawcett, P. A. Rafter, M. A. Weigand, and J.-L. Tison (2014), New insights into sea ice nitrogen biogeochemical dynamics from the nitrogen isotopes, *Global Biogeochem. Cycles*, *28*, doi:10.1002/2013GB004729.

Fripiat, F., D. M. Sigman, G. Massé, and J.-L. Tison (2015), High turnover rates indicated by changes in the fixed N forms and their stable isotopes in Antarctic landfast sea ice, *J. Geophys. Res. Oceans*, *120*, 3079–3097, doi:10.1002/2014JC010583.

Fuhrman, J. A., and D. G. Capone (1991), Possible biogeochemical consequences of ocean fertilization, *Limnol. Oceanogr.*, *36*(8), 1951–1959.

Goreau, T. J., W. A. Kaplan, S. C. Wofsy, M. B. McElroy, F. W. Valois, and S. W. Watson (1980), Production of NO2 and N2O by nitrifying bacteria at reduced concentrations of oxygen, *Appl. Environ. Microbiol.*, *40*, 526–532.

Granger, J., D. M. Sigman, J. A. Needoba, and P. J. Harrison (2004), Coupled nitrogen and oxygen isotope fractionation of nitrate during assimilation by cultures of marine phytoplankton, *Limnol. Oceanogr.*, *49*(5), 1763–1773.

Granger, J., D. M. Sigman, M. M. Rohde, M. T. Maldonado, and P. D. Tortell (2010), N and O isotope effects during nitrate assimilation by unicellular prokaryotic and eukaryotic plankton cultures, *Geochim. Cosmochim. Acta*, *74*, 1030–1040.

Jouandet, M. P., S. Blain, N. Metzl, C. Brunet, T. W. Trull, and I. Obernosterer (2008), A seasonal carbon budget for a naturally iron-fertilized bloom over the Kerguelen Plateau in the Southern Ocean, *Deep Sea Res., Part II*, *55*, 856–867, doi:10.1016/j.dsr.2.2007.12.037.

Karsh, K. L., J. Granger, K. Kritee, and D. M. Sigman (2012), Eukaryotic Assimilatory nitrate reductase fractionates N and O isotopes with a ratio near unity, *Environ. Sci. Technol.*, *46*, 5727–5735.

Kirk, J. T. O. (1992), The nature and measurement of the light environment in the Ocean, in *Primary Productivity and Biogeochemical Cycles in the Sea*, edited by P. G. Falkowski and A. D. Woodhead, Plenum Press, New York and London.

Knapp, A. N., D. M. Sigman, F. Lipschultz, A. B. Kustka, and D. G. Capone (2011), Interbasin isotopic correspondence between upper-ocean bulk DON and subsurface nitrate and its implications for marine nitrogen cycling, *Global Biogeochem. Cycles*, *25*, GB4004, doi:10.1029/2010GB003878.

Laurenceau, E. C., et al. (2015), The relative importance of phytoplankton aggregate and zooplankton fecal pellets to carbon export: Insights from free-drifting sediment trap deployments in naturally iron-fertilized waters near the Kerguelen plateau, *Biogeosciences*, *12*, 1007–1027.

Lehmann, M. F., D. M. Sigman, and W. M. Berelson (2004), Coupling the $^{15}N/^{14}N$ and $^{18}O/^{16}O$ of nitrate as a constraint on benthic nitrogen cycling, *Mar. Chem.*, *88*, 1–20.

Lipschultz, F., S. C. Wofsy, B. B. Ward, L. A. Codispoti, G. Friedrich, and J. W. Elkins (1991), Bacterial transformations of inorganic nitrogen in the oxygen-deficient waters of the eastern Tropical South Pacific Ocean, *Deep Sea Res.*, *37*(10), 1513–1541.

Löscher, C. R., A. Kock, M. Könneke, J. LaRoche, H. W. Bange, and R. A. Schmitz (2012), Production of oceanic nitrous oxide by ammonia-oxidizing archaea, *Biogeosciences*, *9*, 2419–2429.

Malits, A., U. Christaki, I. Obernosterer, and M. G. Weinbauer (2014), Enhanced viral production and virus-mediated mortality of bacterioplankton in a natural iron-fertilized bloom event above the Kerguelen Plateau, *Biogeosciences*, *11*, 6739–6753.

Marconi, D., M. A. Weigand, P. A. Rafter, M. R. McIlvin, M. Forbes, K. L. Casciotti, and D. M. Sigman (2015), Nitrate isotope distribution on the U.S. GEOTRACES North Atlantic cross-basin section: Signals of polar nitrate sources and low latitude nitrogen cycling, *Mar. Chem.*, doi:10.1016/j.marchem.2015.06.007, in press.

Maritorena, S., and D. A. Siegel (2005), Consistent Merging of Satellite Ocean Colour Data Sets using a bio-optical model, *Remote Sens. Environ.*, *94*, 429–440.
Martens-Habbena, W., P. M. Berube, H. Urakawa, J. R. de la Torre, and D. A. Stahl (2009), Ammonia oxidation kinetics determine niche separation of nitrifying Archaea and Bacteria, *Nature*, *461*, doi:10.1038/nature08465.
Martin, J. H., R. M. Gordon, and S. E. Fitzwater (1990), Iron in Antarctic waters, *Nature*, *345*, 156–158.
Mitchel, B. G., E. A. Brody, O. Holm-Hansen, C. McClain, and J. Bishop (1991), Light limitation of phytoplankton biomass and macronutrient utilization in the Southern Ocean, *Limnol. Oceanogr.*, *36*, 1662–1677.
Möbius, J. (2013), Isotope fractionation during nitrogen remineralization (ammonification): Implications for nitrogen isotope biogeochemistry, *Geochim. Cosmochim. Acta*, *105*, 422–432.
Mongin, M., E. Molina, and T. W. Trull (2008), Seasonality and scale of the Kerguelen plateau phytoplankton bloom: A remote sensing and modeling analysis of the influence of natural iron fertilization in the Southern Ocean, *Deep Sea Res., Part II*, *55*, 880–892.
Morel, A., Y. Huot, B. Gentili, P. J. Werdell, S. B. Hooker, and B. A. Franz (2007), Examining the consistency of products derived from various ocean color sensors in open ocean (Case 1) waters in the perspective of a multisensor approach, *Remove Sens. Environ.*, *111*, 69–88.
Mosseri, J., B. Quéguiner, L. Armand, and V. Cornet-Barthaux (2008), Impact of iron on silicon utilization by diatoms in the Southern Ocean: A case study of Si/N cycle decoupling in a naturally iron-enriched area, *Deep Sea Res., Part II*, *55*, 801–819.
Nelson, D. M., et al. (2002), Vertical budgets for organic carbon and biogenic silica in the Pacific sector of the Southern Ocean, 1996–1998, *Deep Sea Res., Part II*, *49*, 1645–1674.
Newell, S. E., A. R. Babbin, A. Jayakumar, and B. B. Ward (2011), Ammonia oxidation rates and nitrification in the Arabian Sea, *Global Biogeochem. Cycles*, *25*, GB4016, doi:10.1029/2010GB003940.
Ogawa, H., R. Fukuda, and I. Koike (1999), Vertical distributions of dissolved organic carbon and nitrogen in the Southern Ocean, *Deep Sea Res., Part I*, *46*, 1809–1826.
Olson, R. J. (1981), The 15 N tracer studies of the primary nitrite maximum, *J. Mar. Res.*, *39*(2), 203–238.
Orsi, A. H., T. Whitworth III, and W. D. Nowlin Jr. (1995), On the meridional extent and fronts of the Antarctic Circumpolar Current, *Deep Sea Res., Part I*, *42*(5), 641–673.
Park, Y.-H., J.-L. Fuda, I. Durand, and A. C. Naveira Garabato (2008a), Internal tides and vertical mixing over the Kerguelen Plateau, *Deep Sea Res., Part II*, *55*, 582–593.
Park, Y.-H., F. Roquet, I. Durand, and J.-L. Fuda (2008b), Large-scale circulation over and around the northern Kerguelen Plateau, *Deep Sea Res., Part II*, *55*, 566–581.
Park, Y.-H., J. H. Lee, I. Durand, and C. S. Hong (2014), Validation of the Thorpe scale-derived diffusivities against microstructure measurements in the Kerguelen region, *Biogeosciences*, *11*, 6927–6937, doi:10.5194/bdg-11-6927-2014.
Planchon, F., D. Ballas, A.-J. Cavagna, A. R. Bowie, D. Davies, T. Trull, E. C. Laurenceau-Cornec, P. Van Der Merwe, and F. Dehairs (2015), Carbon export in the naturally iron-fertilized Kerguelen area of the Southern Ocean based on the ^{234}Th approach, *Biogeosciences*, *12*, 3831–3848.
Pondaven, P., O. Ragueneau, P. Tréguer, A. Hauvespre, L. Dezileau, and J.-L. Reyss (2000), Resolving the "opal paradoxe" in the Southern Ocean, *Nature*, *405*, 168–172.
Rafter, P. A., P. J. DiFiore, and D. M. Sigman (2013), Coupled nitrate nitrogen and oxygen isotopes and organic matter remineralization in the Southern and Pacific Oceans, *J. Geophys. Res. Oceans*, *118*, 4781–4794, doi:10.1002/jgrc.20316.
Santoro, A. E., and K. L. Casciotti (2011), Enrichment and characterization of ammonia-oxidizing archaea from the open ocean: Phylogeny, physiology and stable isotope fractionation, *ISME J.*, *5*, 1796–1808.
Sarmiento, J. L., N. Gruber, M. A. Brzezinski, and J. P. Dunne (2004), High-latitude controls of thermocline nutrients and low latitude biological productivity, *Nature*, *427*, 56–60.
Sarthou, G., D. Vincent, U. Christaki, I. Obernosterer, K. R. Timmermans, and C. P. D. Brussaard (2008), The fate of biogenic iron during a phytoplankton bloom induced by natural fertilization: Impact of copepod grazing, *Deep Sea Res., Part II*, *55*, 734–751.
Savoye, N., T. W. Trull, S. H. M. Jacquet, J. Navez, and F. Dehairs (2008), The ^{234}Th-based export fluxes during a natural iron fertilization experiment in the Southern Ocean (KEOPS), *Deep Sea Res., Part II*, *55*, 841–855.
Sigman, D. M., M. A. Altabet, D. C. McCorkle, R. Francois, and G. Fischer (1999), The δ^{15}N of nitrate in the Southern Ocean: Consumption of nitrate in surface waters, *Global Biogeochem. Cycles*, *13*(4), 1149–1166, doi:10.1029/1999GB900038.
Sigman, D. M., K. L. Casciotti, M. Andreani, C. Barford, M. Galanter, and J. L. Böhlke (2001), A bacterial method for the nitrogen isotopic analysis of nitrate in seawater and freshwater, *Anal. Chem.*, *73*, 4145–4153.
Sigman, D. M., J. Granger, P. J. DiFiore, M. M. Lehmann, R. Ho, G. Cane, and A. van Green (2005), Coupled nitrogen and oxygen isotope measurements of nitrate along the eastern North Pacific margin, *Global Biogeochem. Cycles*, *19*, GB4022, doi:10.1029/2005GB002458.
Sigman, D. M., P. J. DiFiore, M. P. Hain, C. Deutsch, Y. Wang, D. M. Karl, A. N. Knapp, M. F. Lehmann, and S. Pantoja (2009), The dual isotopes of deep nitrate as a constraint on the cycle and budget of oceanic fixed nitrogen, *Deep Sea Res., Part I*, *56*, 1419–1439.
Sigman, D. M., M. P. Hain, and G. H. Haug (2010), The polar ocean and glacial cycles in atmospheric CO_2 concentration, *Nature*, *466*, 47–55, doi:10.1038/nature09149.
Smart, S. M., S. E. Fawcett, S. J. Thomalla, M. A. Weigand, C. J. C. Reason, and D. M. Sigman (2015), Isotopic evidence for nitrification in the Antarctic winter mixed layer, *Global Biogeochem. Cycles*, *29*, 427–445, doi:10.1002/2014GB005013.
Smith, J. M., F. P. Chavez, and C. A. Francis (2014), Ammonium uptake by phytoplankton regulates nitrification in the Sunlit Ocean, *PLoS One*, *9*(9), e108173, doi:10.1371/journal.pone.0108173.
Sokolov, S., and S. R. Rintoul (2007), On the relationship between fronts of the Antarctic Circumpolar Current and surface chlorophyll concentration in the Southern Ocean, *J. Geophys. Res.*, *112*, C07030, doi:10.1029/2006JC004072.
Trull, T. W., D. Davies, and K. Casciotti (2008), Insights into nutrient assimilation and export in naturally iron-fertilized waters of the Southern Ocean from nitrogen, carbon, and oxygen isotopes, *Deep Sea Res., Part II*, *55*, 820–840.
Trull, T. W., et al. (2015), Chemometric perspectives on plankton community responses to natural iron fertilization over and downstream of the Kerguelen plateau in the Southern Ocean, *Biogeosciences*, *12*, 1029–1056.
Ward, B. B. (2007), Nitrification in marine systems, in *Nitrogen in the Marine Environment*, edited by D. G. Capone et al., pp. 199–261, Elsevier, Amsterdam.
Yool, A., A. J. Martin, C. Fernandez, and D. R. Clark (2007), The significance of nitrification for oceanic new production, *Nature*, *447*, doi:10.1038/nature05885.
Yoshiba, N., H. Morimoto, H. Hirano, M. Koike, I. Matsuo, S. Wada, E. A. Saino, and A. Hattori (1989), Nitrification rates and ^{15}N abundances of N_2O and NO_3^- in the western North Pacific, *Nature*, *342*, 895–897.